bioengineering

MDPI

Article

An Autologous Dermal–Epidermal Composite Engineered Skin Repairs Wounds in a Pig Model

Ilia Banakh [1,2], Md. Mostafizur Rahman [1,2], Carlos Luis Arellano [1,2], Phoebe Ang [1], Denese Carol Marks [3], Samantha Lee Williams Warren [4], Cheng Hean Lo [1,2], Heather Cleland [1,2] and Shiva Akbarzadeh [1,2,*]

1 Skin Bioengineering Laboratory, Victorian Adult Burns Service, Alfred Care Group, Bayside Health, 55 Commercial Road, Melbourne, VIC 3004, Australia; ilia.banakh@monash.edu (I.B.); mostafiz.rahman@monash.edu (M.M.R.); carlos.arellano1@monash.edu (C.L.A.); phoebe.ang@monash.edu (P.A.); cheng.lo@monash.edu (C.H.L.); h.cleland@alfred.org.au (H.C.)
2 Department of Surgery, Monash University, 99 Commercial Road, Melbourne, VIC 3004, Australia
3 Australian Red Cross Lifeblood, 17 O'Riordan Street, Alexandria, NSW 2015, Australia; dmarks@redcrossblood.org.au
4 Monash Micro Imaging, Monash University, 99 Commercial Road, Melbourne, VIC 3004, Australia; samantha.warren@monash.edu
* Correspondence: shiva.akbarzadeh@monash.edu; Tel.: +61-3-99030-284; Fax: (+61)-3-9076-6938

Abstract

(1) Background: Meshed split skin grafting (SSG) still remains the gold standard of care for deep wound treatment. The aim of this study was to evaluate an autologous bioengineered dermal–epidermal composite skin for treating full-thickness wounds in a porcine model using a clinically relevant two-stage grafting approach. (2) Methods: Multiple full-thickness wounds were created on the dorsal sites of animals. Wounds were initially grafted with a polyurethane dermal template, followed three weeks later by either Platelet hydroGel–Pig Skin Equivalent (PG-PSE) or meshed SSG control. Human platelet lysate was also assessed as a substitute for foetal calf serum during skin maturation. (3) Results: By two weeks post-grafting, epidermisation of PG-PSE-treated wounds were comparable to SSG-treated wounds. EdU labelling confirmed early engraftment and contribution of graft-derived cells to both neo-epidermis and neo-dermis. Cytokeratin 5+ immunofluorescence staining, showed a hyperproliferative neo-epidermis, enriched in progenitor keratinocytes, typical of early-stage skin grafts in pigs. Neo-dermis was marked with abundance of vimentin^{+} fibroblasts and rete ridges indicating a mature dermal–epidermal junction. Robust neovascularisation was observed in both superficial and deep neo-dermis, with platelet lysate-matured grafts showing greater microvessel formation in superficial neo-dermis in comparison with native skin. Picrosirius red staining of the superficial neo-dermis revealed a lower abundance of thick, red collagen fibres in PG-PSE grafts compared to SSGs, consistent with ongoing collagen deposition and tissue integration in PG-PSE. However, the ratio of thin green collagen fibres to thick red collagen fibres in the deep neo-dermis was largely comparable between group conditions, suggesting that bioengineered grafting does not alter dermal template maturation. (4) Conclusion: Overall, autologous dermal–epidermal bioengineered skin effectively vascularises and repairs wounds over a dermal template. Platelet lysate is a promising alternative to foetal calf serum, although PG-PSE may require longer time for complete dermal maturation and warrants further long-term evaluation.

Keywords: wound and injuries; bioengineering; skin grafting; pig model; keratinocytes; fibroblasts

Check for updates

Academic Editor: Steven Paul Nistico

Received: 1 October 2026
Revised: 1 November 2026
Accepted: 2 November 2026
Published: 4 November 2026

Copyright: © 2026 by the authors. Licensee MDPI, Basel, Switzerland. This article is an open access article distributed under the terms and conditions of the Creative Commons Attribution (CC BY) license.

1. Introduction

Anatomic and physiological similarities of humans and pigs make porcine skin a commonly studied and valuable wound repair model. Epidermal thickness in pigs (30 to 140 μm) is similar to that in humans (50 to 120 μm) and both epidermises present with well-developed dermal rete ridges, sub-dermal adipose tissue and sparse body hair. In addition, both species manifest a comparable skin blood vessel network [1,2]. Importantly, similar to humans, pig skin wounds are repaired with re-epidermisation, whereas rodents heal mostly via wound contraction.

In order to test engineered skin grafts in pigs, two approaches have been adapted: grafting human-derived engineered skin to an immunosuppressed pig [3], or grafting an autologous porcine engineered skin [4,5]. The latter was chosen in this study, providing the advantage of a physiologically relevant graft integration and remodelling in a fully immunocompetent animal.

Our group has previously shown that a dermal–epidermal composite skin can be prepared by seeding human fibroblasts and keratinocytes into a hydrogel made from human platelet material. The bioengineered skin, a Platelet hydrogel–Human Skin Equivalent (PG-HSE), presented with similar architecture and features to human native skin [6]. We have demonstrated effective wound closure by grafting PG-HSE in immune-compromised nude mice [7]. The contribution of grafted keratinocytes to wound closure in this xenograft model was shown using human-specific antibodies.

One of the challenges in creating a holistic wound healing model is the ability to track the cells that close the wound as a result of the intervention. In this study, in vitro DNA labelling using thymidine analogues was used to trace the autologous engineered skin post-grafting in pigs. Although this method has been effective in tracking injected autologous mesenchymal stem cells and fibroblasts post-grafting in pigs [8,9], keratinocyte tracking in neo-epidermis has not been reported before. We investigated epidermisation and full-thickness wound closure using 5-Ethynyl-2′-deoxyuridine (EdU)-labelled autologous engineered skin in a two-stage surgical procedure.

The two-stage skin grafting in pigs reflects the clinical treatment of deep wounds [10]. To simulate real life clinical conditions, large full-thickness wounds were initially grafted with a dermal template, which is vascularised over time, providing a robust wound bed. During this period, autologous, engineered skin was constructed through minor modifications of the methods used to produce the human version of the bioengineered skin, PG-HSE, to form a Platelet hydroGel Porcine Skin Equivalent (PG-PSE). Similarly to the human version, PG-PSE incorporated autologous basal keratinocytes and dermal fibroblasts in a novel Platelet hydroGel (PG) as the scaffold. Grafts were labelled with EdU, and the labelled composite dermal–epidermal composite skin was grafted to close wounds. Epidermisation, vascularisation and collagen composition were then examined. The current study provided a pig model to test the autologous bioengineered composite skin against the gold-standard native meshed split skin graft (SSG), in a clinically relevant manner.

2. Materials and Methods

2.1. Isolation and Expansion of Porcine Keratinocytes and Dermal Fibroblasts

Fresh skin was processed to isolate pig fibroblasts and keratinocytes as described for human skin previously, with minor modifications (9). Isolated fibroblasts were expanded in fibroblast medium containing low glucose Dulbecco's Modified Eagle Medium (DMEM) with 4% foetal bovine serum (FBS, Cytiva, Melbourne, Australia), hydrocortisone (0.5 μg/mL, Millipore, Burlington, MA, USA), insulin (50 IU/mL, Merck, Melbourne, Australia), EGF (10 ng/mL, R&D Systems, Minneapolis, MN, USA) and gentamicin (50 μg/mL, Thermo Fisher Scientific, Melbourne, Australia). Epidermal sheets were

digested with trypsin (0.25%, Thermo Fisher Scientific, Australia) at 37 °C for 5–7 min to release the basal keratinocytes. Keratinocytes were expanded on irradiated feeder cells CCL92 (ATCC, Manassas, VA, USA) in cFAD medium: DMEM and Ham's F12 (3:1 ratio, Life Technologies, Australia), L-Glutamine (4 mM, Life Technologies, Australia), adenine (0.18 mM, Merck, Australia), hydrocortisone (0.4 µg/mL), insulin (5µg/mL), 3,3′,5-triiodo-L-thyronine sodium salt (2×10^{-9} M, Sigma-Aldrich, Melbourne, Australia), transferrin (5 µg/mL, Sigma-Aldrich, Australia), gentamicin (50 µg/mL), isoproterenol (0.2 µg/mL, Hospira, Melbourne, Australia), EGF (10 ng/mL), and 10% FBS.

2.2. EdU/BrdU Labelling Optimisation in Monolayer

Porcine keratinocytes were seeded on irradiated feeder cells in chambered slides (Sarstedt, Adelaide, Australia). Porcine fibroblasts were directly seeded on chamber slides. Once attached, cells were fed with 10 µM EdU (Invitrogen, Melbourne, Australia) or 10 µM BrdU (Sigma-Aldrich, Australia) in culture medium for 48 h. Afterwards, cells were tracked for label retention and stained on days 3, 8 and 16 post-labelling.

2.3. Preparation of Platelet Hydrogel–Pig Skin Equivalent (PG-PSE)

PG hydrogel scaffolds were prepared as previously reported with some modifications (6). Briefly, 2.4 IU/mL thrombin was added to human platelet precipitate (Australian Red Cross Lifeblood, Alexandria, NSW, Australia) to form a hydrogel. Expanded porcine dermal fibroblasts were seeded at $0.25 \times 10^6/cm^2$, 24 h post-gelation, and left for 72 h to spread over PG scaffold in submerged culture. This was followed by seeding of basal keratinocytes ($0.5 \times 10^6/cm^2$). PG-PSEs were grown at the air–liquid interface in UCDM1 maturation medium consisting of low glucose DMEM (Thermo Fisher Scientific, Australia) 1:1 with Ham's F12 medium (Thermo Fisher Scientific, Australia) plus L-glutamine (4.5 mM), L-serine (1.5 mM, Sigma-Aldrich, Australia), CaCl2, (1 mM Sigma-Aldrich, Australia), adenine (1.8 mM), O-phosphoryl ethanolamine (5 µM, Sigma-Aldrich, Australia), gentamicin (50 µg/mL), strontium chloride (1 mM, Sigma-Aldrich, Australia), 1 × ITS (Sigma-Aldrich, Australia), linoleic acid (10 µg/mL, Sigma-Aldrich, Australia), ascorbic acid (0.1 mM, Sigma-Aldrich, Australia), 3,3′,5-triiodo-L-thyronine sodium salt (2×10^{-12} M), hydrocortisone (0.5 µg/mL), KGF (5 ng/mL, R&D Systems, Minneapolis, MN, USA), EGF (10 ng/mL) and FGF-2 (1 ng/mL, R&D Systems, Minneapolis, MN, USA) with 0.3% FBS (serum-supplemented) or 0.2% platelet lysate (serum-free) for five days.

To label 3D PG-PSEs, fresh UCDM1 culture medium was supplemented with 10 µM EdU and added to the PG-PSE cultures 48 h before surgery. PG-PSEs were washed in fresh low glucose DMEM, supplemented with amphotericin/gentamicin prior to surgery and transported to the animal operating theatre for grafting.

2.4. Animal Surgery

A total of five 2–3-month-old, female, large white pigs (*S. domesticus*) were sedated and transported to the surgical theatre. An endotracheal tube was inserted and isoflurane anaesthesia administered through a face mask (2–3.5% isoflurane per litre), with Buprenorphine (0.01 mg/kg i.v.) injected for perioperative pain management. Pigs were placed in sternal recumbency on the operating table. Anaesthetic delivery, and vital signs were continuously monitored. During the initial surgery, a 7 × 7 cm full-thickness donor skin was recovered under aseptic conditions to prepare PG-PSE. The wound was grafted with Novosorb® biodegradable temporising matrix (BTM) as a dermal template (PolyNovo, Melbourne, Australia) and dressings were applied. Fentanyl ear patches (Apotex, Sydney, Australia) were provided for postoperative pain management.

A week after taking donor skin, seven full-thickness wounds were created on the dorsal side of each pig (Supplementary Data S1). Wounds were grafted with BTM as described above. The animals underwent routine dressing changes twice weekly, while PG-PSE autografts were prepared. It has been shown by others that BTM is fully integrated in three weeks in young pigs [11]. After three weeks, the temporary seal of the BTM was removed, and wounds were splinted to minimise infiltration of the host epidermis. The seven wounds were grafted with a randomised allocation of 3 serum-free PG-PSEs, 3 serum-containing PG-PSEs and 1 meshed SSG per pig. A wound chamber was tested on one wound per graft type (i.e., 1 out of 3) in two pigs to create a barrier against epidermisation from the wound margins. Skin grafts were secured in place over the vascularised wound bed and held in place on the edges using sutures with Conformant 2 wound veil (Smith & Nephew, Melbourne, Australia) backing.

Dressings were applied over each grafted wound in the following sequence: Mepitel (Mölnlycke Health Care, Sydney, Australia), wet gauze (soaked in PBS with 50 ug/mL gentamicin and 1 ug/mL amphotericin B), Combine (Mediflex, Sydney, Australia), Conformant 2, Tegaderm (Solventum, Melbourne, Australia), Opsite (Smith & Nephew, Melbourne, Australia), Hypafix (BSN Medical, Hamburg, Germany), and Exu-dry (Smith & Nephew, Australia). VetRap (Solventum, Melbourne, Australia) and a body coat were fitted for graft protection. Tissue samples were collected from the middle of the grafts using an 8 mm punch biopsy at week 1 and week 2 after skin grafting for processing and assessment. At each surgery and dressing change, standardised photographs were taken to assess healing, total wound size reduction, graft survival, and presence of infection by comparison with the baseline values. On Day 14, pigs were humanely euthanised. All wounds were excised and taken to the lab for processing and analysis.

2.5. Histological Staining

Skin graft biopsies were fixed in 4% paraformaldehyde prior to cryopreservation. Specimens were sectioned and stained with haematoxylin and eosin as previously described (9). For Masson's trichrome staining, sections were processed according to standard protocols as previously described (9). Whole stained sections (6 mm punch biopsy) were imaged using a Nikon Eclipse Ts2 inverted microscope (10×/0.30 objective) and Nikon DS-Fi3 camera. An Image J macro (NIH) was used to quantify collagen by assigning thresholds for the following colours: black (0–8), blue (120–177, collagen) and purple (178–220). Collagen was quantified separately in the superficial and deep neo-dermis. Superficial neo-dermis was determined as areas directly below the epidermis (within 200 µm of dermoepidermal junction), while deep neo-dermis encompassed lower areas directly above BTM (>600 µm below dermoepidermal junction). Six randomly selected regions of 360 × 240 µm size within the superficial and deep neo-dermis were selected for collagen analysis. Results from all grafts per treatment group in each pig were averaged and one-way ANOVA statistical method was applied to compare grafts.

For collagen composition, 6 mm punch biopsy sections were stained with Picrosirius red (Abcam, Cambridge, UK) and imaged using an Olympus VS200 slide scanner under polarised light at 20× magnification. A modified ImageJ macro (PR-BRF Analyser v2.20, CCM Lab, Darlinghurst, NSW, Australia) was used to measure areas occupied by each colour [12]. Images were converted to 8-bit with colour ranges assigned to collagen fibre types as follows: red (0–27, 240–255, long/mature), yellow (28–47, mixed/intermediate), and green (48–140, thin), with the brightness minimum and saturation minimum thresholds both set to 10 to match background noise when compared to an unstained control. Colour thresholds reflect controls including collagen I, native human skin, and native porcine skin. Five randomly selected regions of 360 × 240 µm each within the superficial and deep

neo-dermis were selected and analysed for collagen composition. Data from all wounds per treatment group in each pig were averaged and two-way ANOVA statistical method was applied to compare grafts.

2.6. Immunofluorescence

Fixed tissue sections or cells were permeabilised in with 0.2% (*v*/*v*) Triton X-100 (Sigma, Australia) for 10 min and washed in PBS. Sections were blocked using 3% normal goat serum or normal donkey serum for 30 min and then washed. Mouse anti-BrdU antibody (1:300, Invitrogen, Australia); rabbit anti-pancytokeratin (1:100, Novus Biologicals, Centennial, CO, USA); mouse anti-pig CD45 (1:200, GeneTex, Irvine, CA, USA); rabbit anti-vimentin (1: 600, Cell Signalling, Danvers, MA, USA), rabbit anti-CD31 (1:100, Abcam, Cambridge, UK) or rabbit anti-cytokeratin 5 (1: 100, BioLegend, San Diego, CA, USA) primary antibody was added to the sections and incubated overnight at 4 °C in a humidified chamber. The primary antibody was washed off and sections were incubated with goat anti-mouse Ig-AF 488 (1:400, Invitrogen, Australia), goat anti-rabbit Ig-AF 488 (1:400, Invitrogen, Australia), donkey anti-mouse Ig-AF568 (1:400, Invitrogen, Australia), donkey anti-rabbit-AF647 (1:400, Invitrogen, Australia) and Hoechst 33342 (1:500) stains for 45 min at room temperature before multiple wash with PBS. Coverslips were mounted coverslips using ProLong Gold solution (Invitrogen, Australia). For BrdU detection, slides were initially pretreated with 4M HCl for 3 min and washed in PBS prior to permeabilisation. For EdU detection, sections were processed as per Click-iT Plus kit instructions (Invitrogen, Australia). Widefield Nikon Ti-E and confocal Nikon A1r microscopes were used to visualise EdU presence in the far-red channel.

Images acquired using an Olympus VS200 slide scanner were analysed using QuPath version 0.7.0 and Fiji/ImageJ version 1.54 to quantify vessel diameter and vessel abundance within the superficial and deep neo-dermal layers.

For CD31 quantification, in QuPath, regions of interest (ROIs) were manually annotated to define the superficial neo-dermis, corresponding to 200 µm of the neo-dermis, and the deep neo-dermis, corresponding to the region directly above the BTM (>600 µm deep). Vessel segmentation was performed in QuPath using the pixel classifier machine-learning tool [13]. Vessel segmentation was performed in QuPath using the pixel classifier machine-learning tool. The classifier was trained to identify a CD31-positive signal, using a representative subset of vessels across thirteen images (3 SSG, 4 native skin, 3 PL and 3 FCS). Segmented objects with a minimum diameter below 3 µm were excluded from downstream analysis. For each ROI, QuPath was used to measure the total annotated area, total CD31-positive vessel area, vessel area fraction, and number of detected vessel objects. Vessel coverage was calculated as

$$\text{Vessel area (\%)} = \text{total CD31-positive segmented vessel area/total ROI area} \times 100.$$

Binary masks of the ROIs and vessel detections were exported from QuPath as TIFF images for vessel diameter analysis in Fiji/ImageJ. Masks were batch-processed using a standardised macro workflow. Each mask was converted to a binary image, skeletonised to reduce each vessel object to its medial axis, and used to generate a Euclidean distance map from the corresponding binary vessel mask. Local vessel diameter was calculated by multiplying the distance map value along the vessel skeleton by two, thereby converting the radius from the medial axis to the vessel boundary into a diameter measurement. Vessel diameter measurements were then summarised for each ROI. Data from all wounds per treatment group in each pig were averaged and one-way ANOVA statistical method was applied to compare grafts.

3. Results

3.1. An Autologous Bioengineered Skin Graft to Treat Full-Thickness Wounds in a Pig Model

In order to test the autologous dermal–epidermal composite bioengineered skin graft, PG-PSE, multiple full-thickness wounds were created on the dorsal side of each young female large white pig (Figure 1A,B). All wounds were grafted with polyurethane-based acellular BTM dermal template. BTM provided a template for vascularisation, cell infiltration and nerve regeneration over three weeks (Figure 1C). Wounds were then grafted with either PG-PSE or traditional meshed SSG as control. PG-PSE was prepared from autologous basal keratinocytes and fibroblasts, which were isolated from pig skin and expanded in the laboratory. Autologous cells were seeded on a Platelet hydroGel (PG) to form the mature PG-PSE. Human platelet lysate (PL) was investigated as an alternative media supplement to foetal bovine serum (FBS) during skin maturation phase. PG-PSE architecture was monitored by Haematoxylin and Eosin staining in vitro, showing similar architecture between PG-PSE matured in serum-free (Figure 2A) and in serum-containing conditions (Figure 2B).

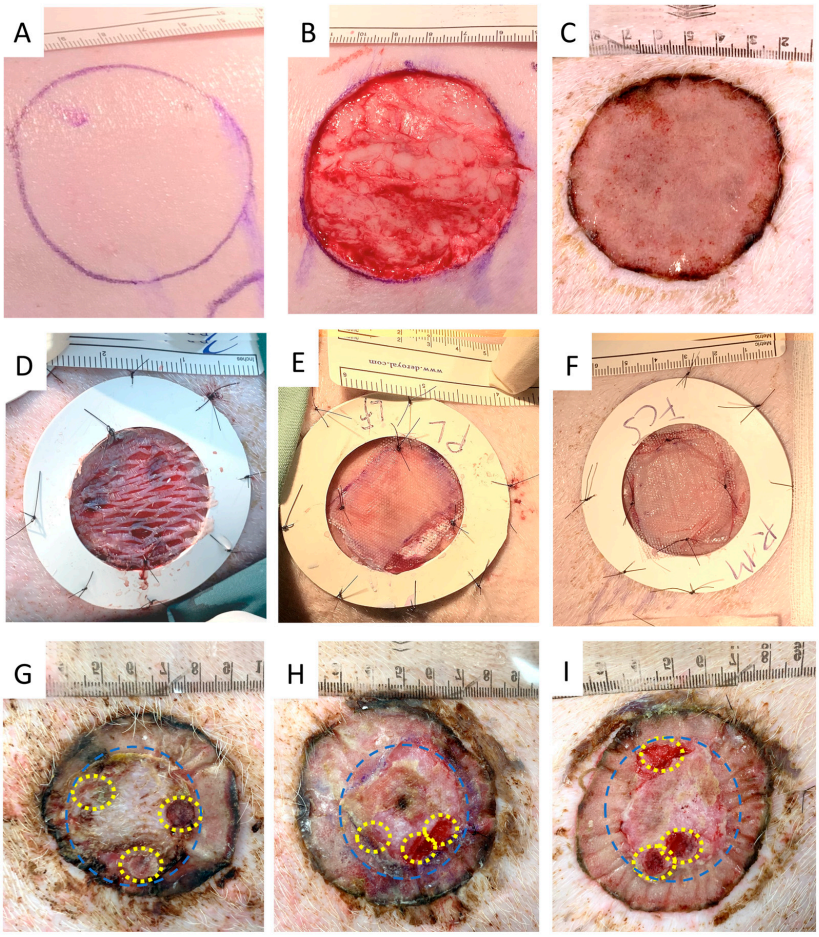


Figure 1. Macroscopic images of Platelet hydrogel–Pig Skin Equivalent. Representative image of (**A**) marked wound area; (**B**) a full-thickness wound; (**C**) Novosorb® BTM temporised wound before skin grafting. (**D**–**F**) Three weeks later, in preparation for grafting, silicone inserts were sutured around each wound. Images of (**D**) meshed SSG, (**E**) PG-PSE, matured in serum-free supplemented media, or (**F**) PG-PSE, matured in serum- supplemented media. Two weeks post-grafting, healed (**G**) SSG; (**H**) Serum-free graft; and (**I**) serum-supplemented graft are shown. Skin grafted area is marked with dashed blue circle. Punch biopsy sites are indicated by dashed yellow lines. N = 5 pigs, 3 grafts per treatment group per animal. Abbreviations: SSG: split skin graft; PG-PSE: Platelet hydroGel–Pig Skin Equivalent.

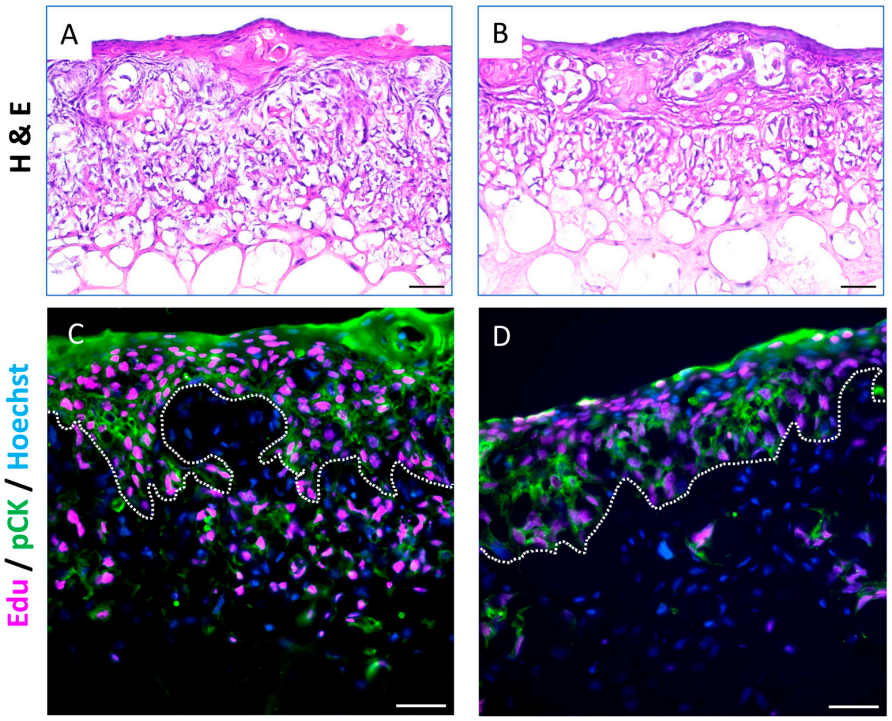


Figure 2. Platelet hydrogel–Pig Skin Equivalent architecture. Dermal–epidermal composite structure was detected by Haematoxylin and Eosin staining when PG-PSE was matured in (**A**) serum-free and (**B**) serum-supplemented maturation media on the day of grafting. Two days prior to grafting, 10 μM EdU was added to both (**C**) serum-free and (**D**) serum-supplemented maturation media to label and track fibroblasts and keratinocytes. pan-cytokeratin (green) was detected by immunofluorescence. Dashed white line marks epidermal–dermal junction (**C**,**D**). N = 5 pigs; 3 grafts per treatment per animal; 2 images per graft. Scale bar: 100 μm. Abbreviations: PG-PSE: Platelet hydroGel–Pig Skin Equivalent.

One out of seven wounds per pig was grafted with traditional meshed SSG, as the gold-standard control group. Three wounds were grafted with autologous PG-PSE either matured in serum-free media or PG-PSE matured in serum-supplemented media (Figure 1D–F). Skin grafts were secured with sutures and several layers of wound dressings to minimise shearing.

Graft integration and wound repair were monitored macroscopically and histologically over the course of 14 days with regular dressing change. On Day 14, grafted areas with autologous bioengineered skin were epidermised (Figure 1H,I), similar to the gold-standard meshed SSG (Figure 1G). No macroscopic differences were observed between the wounds closed with the PG-PSE matured in serum-free (Figure 1H) and serum-supplemented (Figure 1I) media.

3.2. Grafted Keratinocytes Formed a Traceable Neo-Epidermis in Pigs

Both BrdU and EdU thymidine analogues were tested for labelling autologous PG-PSE. Initially, keratinocytes and fibroblasts, were labelled with either a BrdU or EdU in monolayer (Supplementary Data S2). Although both thymidine analogues labelled the cells, to retain and track cells for longer, EdU labelling was performed on the 3D PG-PSE construct prior to grafting. EdU is a small molecule and does not activate T-cell mediated immune response [14,15]. EdU detection is antibody independent and does not rely on DNA denaturation.

EdU-labelled cells were observed throughout the depth of PG-PSE. There appeared to be more labelled cells in the PG-PSE matured under serum-free conditions (Figure 2C) both

in dermis and epidermis, likely due to slower proliferation and turnover of cells, compared to PG-PSE matured in serum-containing conditions on the grafting day (Figure 2D). Seven days post-grafting of PG-PSEs, labelled keratinocytes and fibroblasts were detected in the serum-free (Figure 3B,E) and serum-containing (Figure 3C,F) grafts. The numbers of EdU-labelled cells were reduced post-grafting, possibly due to rapid fibroblast proliferation leading to label dilution in dermis. Similarly, during epidermal turnover, stratified keratinocytes flatten and mature, losing their labelled nuclei and eventually shed off. EdU signals were largely undetected by two weeks post-grafting. An influx of CD45+ scavengers was observed in PG-PSE grafts at week 1 suggesting an active immune-mediated removal of the debris at this early time point.

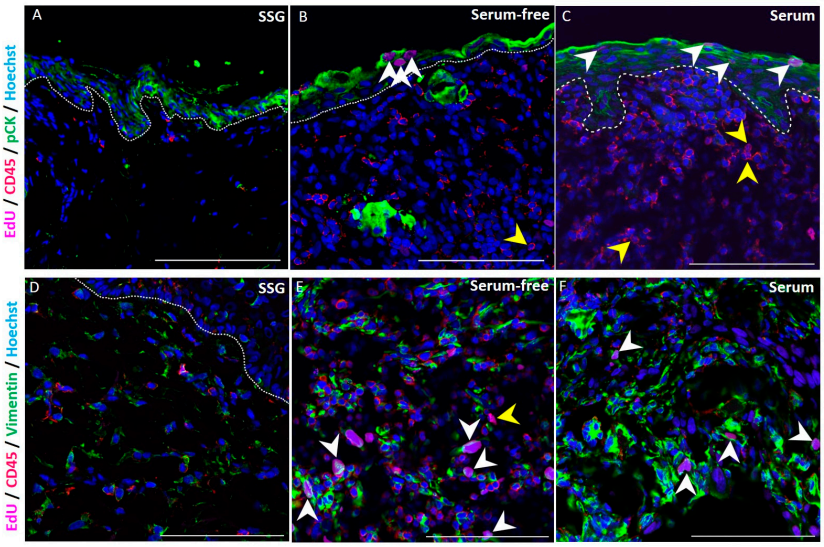


Figure 3. Detection of labelled cells in Pig skin Equivalent post-grafting. (**A**–**C**) At week 1 post-grafting, pan-cytokeratin (green) and CD45 (red) were detected by immunofluorescence. EdU signal was tracked in (**A**) SSG, (**B**) serum-free PG-PSE and (**C**) serum-supplemented PG-PSE and detected in panCK$^+$ keratinocytes (white arrowheads), and CD45$^+$ scavengers (yellow arrowheads). (**D**–**F**) Vimentin (green) and CD45 (red) were also detected by immunofluorescence in neo-dermis at week 1 post-grafting. EdU-label was tracked in (**D**) SSG (**E**) serum-free PG-PSE, (**F**) serum-supplemented PG-PSE and detected in Vimentin$^+$ fibroblasts (white arrowheads) and CD45$^+$ scavengers (yellow arrowheads). N = 5 pigs; 3 grafts per treatment group per animal, 2 images per graft. Scale bar: 100 µm. Abbreviations: SSG: split skin graft; PG-PSE: Platelet hydroGel–Pig Skin Equivalent.

3.3. Bioengineered Skin Graft Forms a Neo-Dermis and Neo-Epidermis Enriched in Progenitor Keratinocytes and Displays Rete Ridge Architecture

Haematoxylin and eosin-stained graft biopsies presented with moderate thickening of the epidermis in meshed SSG. Both PG-PSE graft groups exhibited thicker epidermis, indicative of epidermal hyperplasia, with rete ridge elongations growing deep into dermal space. Hyperplasia was confirmed by immunofluorescent staining using cytokeratin 5 (CK5) antibody. Porcine native skin exhibited CK5 signal confined to the basal keratinocyte layer (Figure 4E). Conversely, in SSG (Figure 4F) and in both serum-free and serum-containing PG-PSE (Figure 4G–H), CK5 signal was detected across the entire thickness of epidermis. A similar outcome was reported by Bruen et al. in mice, that is, their model of EGFP, synthesised under a CK5 promoter, recorded maximum signal in the advancing wound margin re-epithelialisation between days 12 and 15 post-burn injury [16]. In the dermis, signals from vimentin-expressing cells were observed in SSG (Figure 4J) and both PG-PSE grafted regions (Figure 4K,L) when compared to native pig skin (Figure 4I).

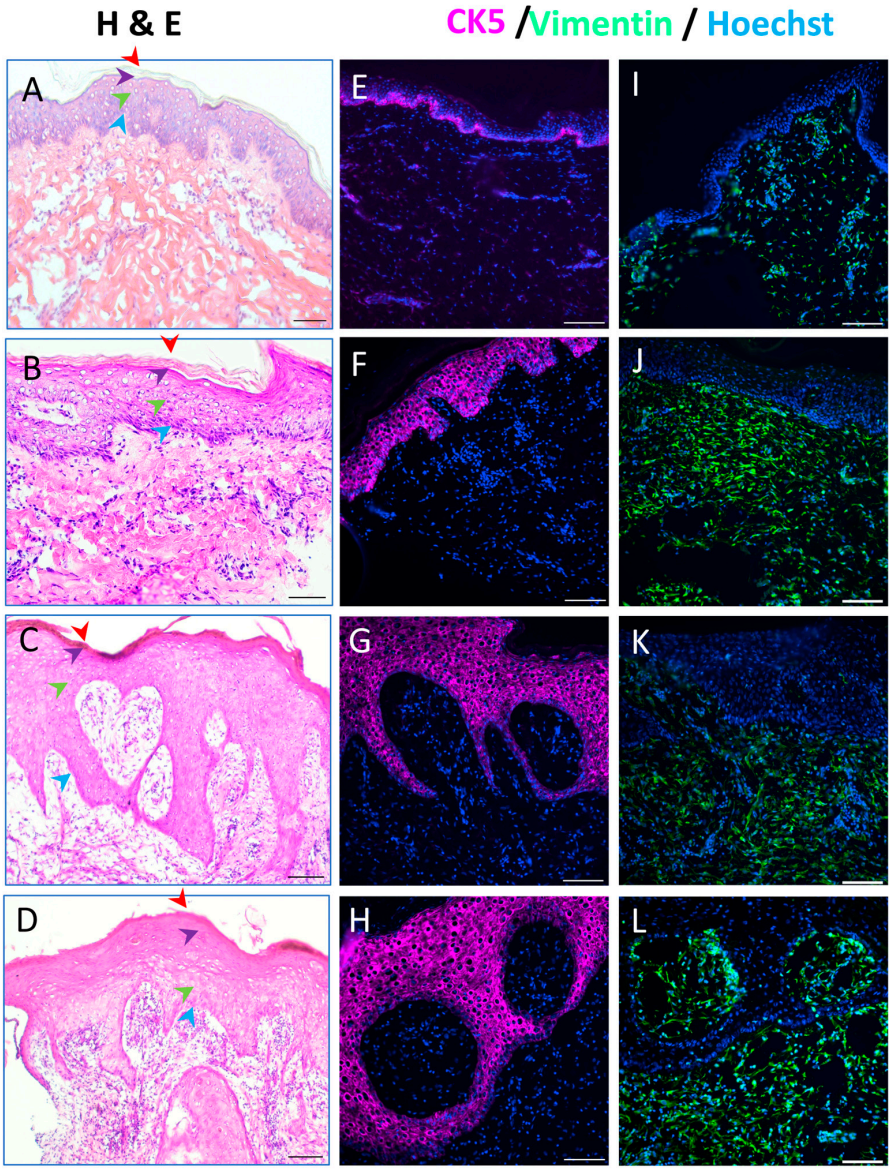


Figure 4. Graft maturation at 2 weeks post-surgery. (**A**,**E**,**I**) Architecture of native pig skin was compared with representative sections from (**B**,**F**,**J**) SSG, (**C**,**G**,**K**) PG-PSE matured in serum-free media and (**D**,**H**,**L**) PG-PSE matured in serum-supplemented media. (**A**) Haematoxylin and Eosin staining of native pig skin, (**B**) SSG, (**C**) PG-PSE matured in serum-free media and (**D**) PG-PSE matured in serum-supplemented media are represented. Arrowheads identify epidermal strata: stratum corneum (red), stratum granulosum (purple), stratum spinosum (green) and stratum basale (blue). Cytokeratin 5 (CK5) expression is restricted to basal layer in (**I**) native pig skin, while spread across whole epidermis in (**F**) SSG control and PG-PSE grafts matured in (**G**) serum-free and (**H**) serum-supplemented media. Fibroblasts were detected in (**I**) native skin and (**J**–**L**) all grafted tissues using vimentin (green) antibody. N = 5 pigs; 3 grafts per treatment group per animal; 2 images per graft. Scale bar: 100 µm. Abbreviations: SSG: split skin graft; PG-PSE: Platelet hydroGel–Pig Skin Equivalent.

3.4. Neovascularisation Supports Bioengineered Skin Graft Survival

Immunofluorescence staining for the endothelial marker CD31 enabled visualisation and quantification of the vascular network within each grafted area. Vessel density and vessel thickness were assessed in the superficial and deep neo-dermis (Figure 5). Numerous microvessels were observed in the superficial neo-dermis at two weeks following skin grafting (Figure 5E). The increased abundance of microvessels relative to uninjured skin

suggests that the grafts remained in an active phase of integration and remodelling at this time point. Wounds grafted with PG-PSE matured in platelet lysate-supplemented medium under serum-free conditions exhibited significantly greater microvessel density in the superficial neo-dermis, immediately beneath the neo-epidermis, compared with uninjured native skin ($p = 0.0461$), indicating that platelet lysate may promote neovascularisation in grafts.

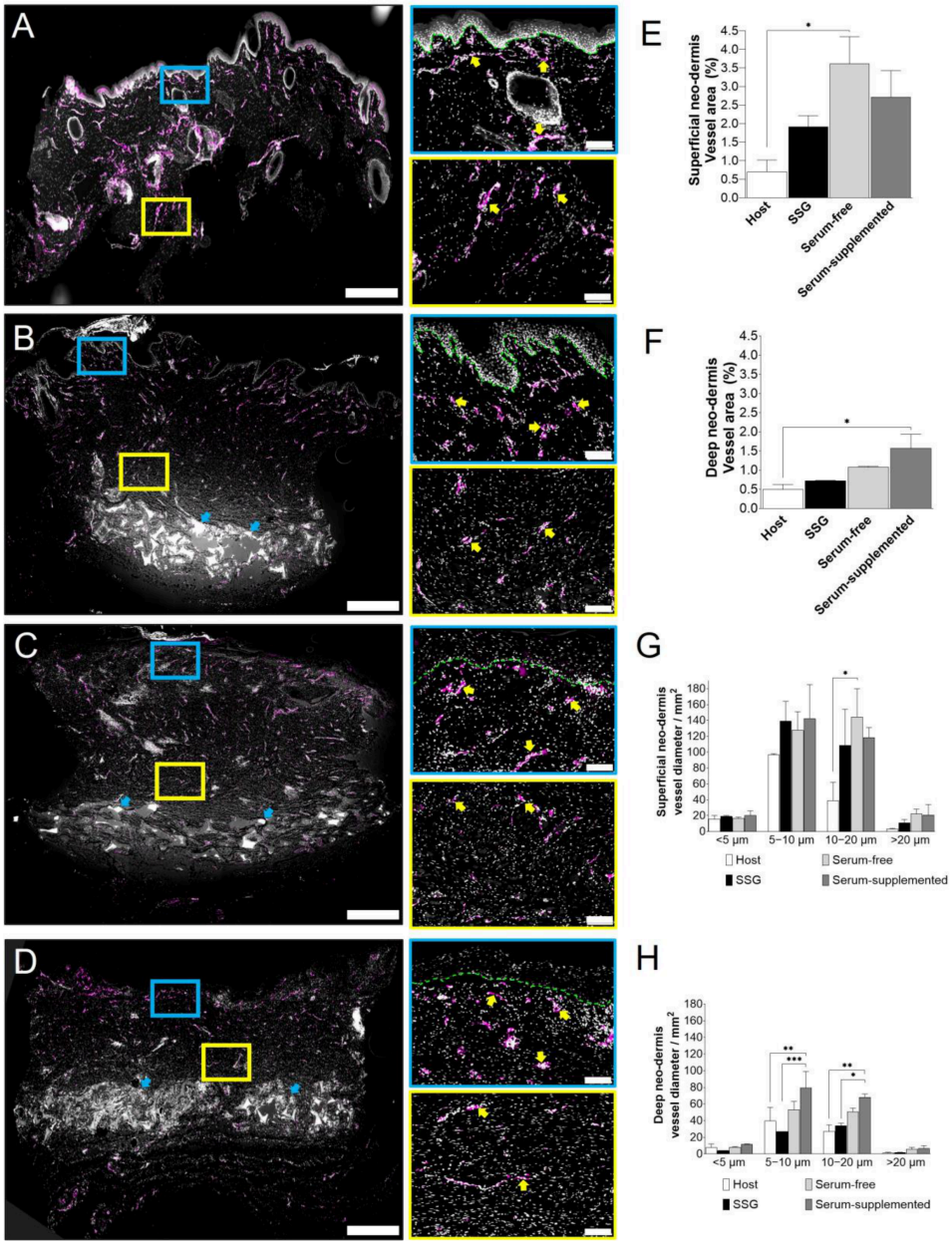


Figure 5. Graft vascularisation. Grafts were analysed with CD31 antibody immunofluorescence at week 2 post-grafting. large scans of (**A**) native pig skin (**B**) SSG; (**C**) PG-PSE grafts matured in serum-free media; and (**D**) PG-PSE grafts matured in serum-supplemented media are represented. Blue arrows mark BTM presence below deep neo-dermis. Zoomed images show superficial (blue outline) and deep (yellow outline) neo-dermis areas at higher resolution. Yellow arrows point out $CD31^+$ vessels. Blood vessel area (%) in (**E**) superficial and (**F**) deep neo-dermis are analysed using two-way ANOVA. Vessel diameter distribution in (**G**) superficial and (**H**) deep neo-dermis are also analysed using two-way ANOVA. $p \leq 0.05$ (*), $p \leq 0.01$ (**), $p \leq 0.001$ (***); N = 2 pigs; 3 grafts per treatment group per animal; whole superficial and deep neo-dermis area in 6 mm punch biopsy per graft. Full scan scale bar: 500 µm. Zoomed images scale bar: 50 µm. Abbreviations: SSG: split skin graft; PG-PSE: Platelet hydroGel–Pig Skin Equivalent.

Most microvessels identified within both the superficial and deep neo-dermis measured between 5 and 20 μm in diameter, with vessels in the 10–20 μm range being the most prevalent. Compared with native skin, PG-PSE superficial neo-dermis matured under serum-free conditions contained significantly more vessels with diameters of 10–20 μm (Figure 5G, $p = 0.0154$). This shift towards larger calibre microvessels may indicate ongoing maturation of the superficial neo-dermal vascular network. Conversely, in deep neo-dermis, PG-HSE matured in serum contained significantly more vessels (5–10 μm diameter, $p = 0.0083$, and 10–20 μm diameter, $p = 0.0068$) compared to native skin (Figure 5F). Notably, residual fragments of the biodegradable temporising matrix (BTM) were still evident within the deep neo-dermis of both SSG- and PG-PSE-treated wounds at five weeks following BTM implantation. This observation is consistent with previous reports demonstrating the relatively slow degradation kinetics of BTM in vivo [17].

3.5. Collagen Deposition and Remodelling

Collagen deposition by dermal fibroblasts was detected with Masson's Trichrome staining two weeks post-skin grafting (i.e., five weeks post-dermal template grafting). In native pig skin, tightly packed, dark blue staining throughout the dermis indicates the presence of dense collagen (Figure 6A). Conversely, relatively loosely packed collagen was observed by form of lighter blue staining in SSG (Figure 6B) and both PG-PSE matured in serum-free (Figure 6C) and serum-supplemented (Figure 6D) media.

Quantification of collagen in the superficial neo-dermis showed SSG contained significantly higher amounts of collagen, as expected, when compared to freshly deposited collagen in both types of PG-PSEs. Collagen density in all native and bioengineered grafts still lagged behind the collagen density of uninjured healthy superficial neo-dermis two weeks post-grafting (Figure 6E). In the deep neo-dermis, there was no significant difference between the amount of collagen deposition in SSG and both types of PG-PSE. However, all three treatment groups had significantly lower collagen deposition when compared to uninjured native pig skin (Figure 6F), providing further evidence that grafts are still in active integration phase at this time point.

Collagen fibre architecture was visualised with Picrosirius red staining, allowing discrimination between freshly deposited green thin fibres and red mature thick fibres, when imaged under polarised light. As expected, mature, red, basket-weave-structured collagen bundles were observed in deep (reticular) native dermis, while some random collagen bundles were present in superficial (papillary) native dermis (Figure 7A).

Both types of collagen fibres, thick/mixed (red and yellow fibres) and thin (green fibres), were detected in uninjured and skin grafts. Notably, significantly higher levels of thick/mixed collagen fibres were observed in the superficial neo-dermis of SSG when compared to both types of PG-PSE grafts (Figure 7E, $p = 0.0027$ for serum-free PG-PSE, $p = 0.0009$ for serum-supplemented PG-PSE). Similar amount of thin collagen fibres was detected in uninjured and all skin grafts. This suggested that unlike native skin grafts, freshly deposited thin collagen fibres contribute proportionately more than the thick/mixed fibres to the total collagen in PG-PSE grafts' superficial neo-dermis. Collagen deposition and integration still outweighs remodelling in superficial neo-dermis two weeks post-grafting compared to SSG.

Conversely, in the deep neo-dermis that was formed over five weeks since the BTM grafting, there was no significant difference observed in collagen fibres between three types of grafts and native skin (Figure 7F). Overall, similar composition and structure in the grafts deep neo-dermis suggests that remodelling in all grafts occurs in a similar fashion, regardless of whether the wounds are closed with SSG or PG-PSE. Five weeks post-grafting, all grafts have reached similar pre-grafting collagen composition in deep neo-dermis.

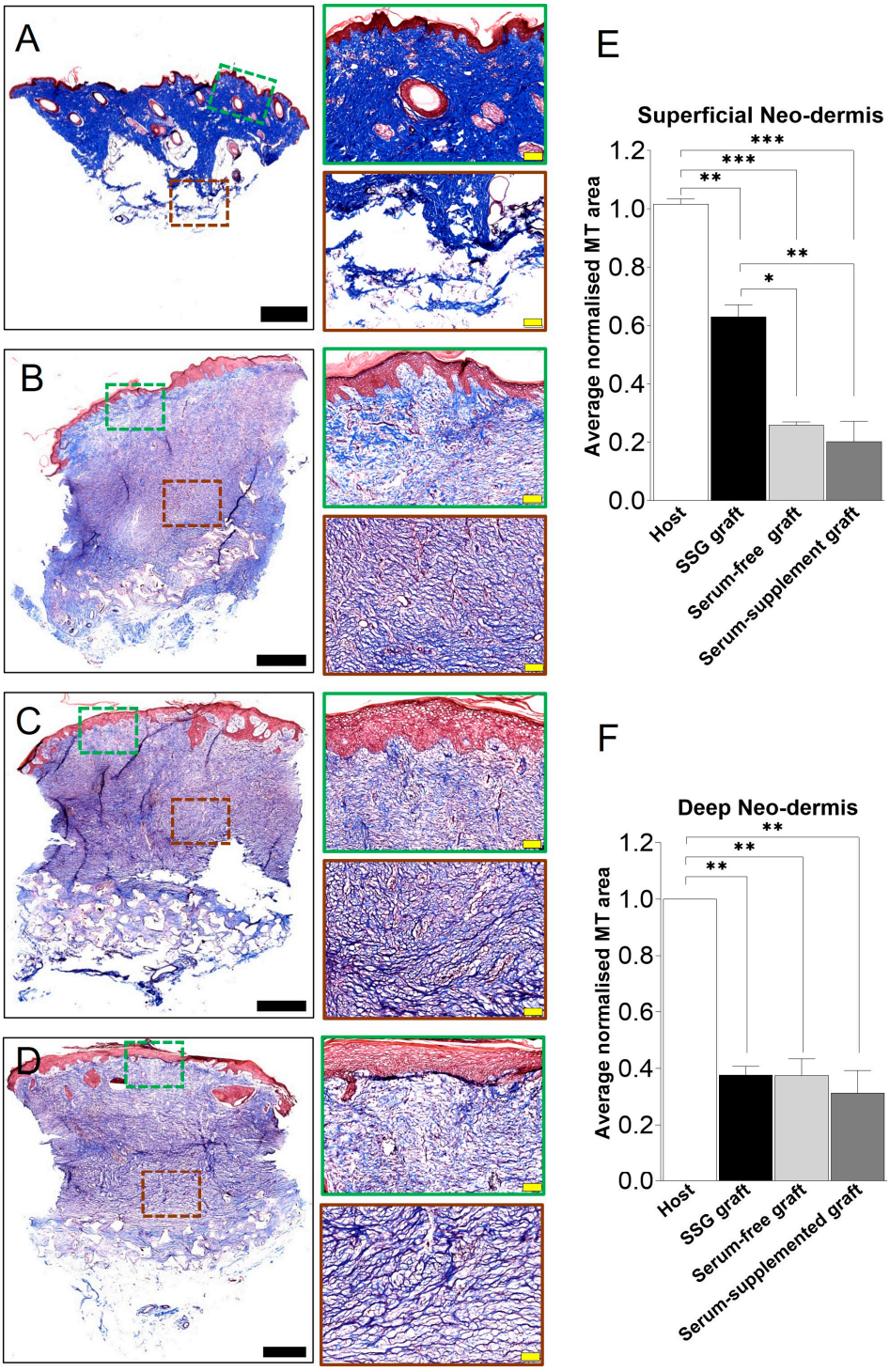


Figure 6. Graft Masson's trichrome (MT) staining at week 2. (**A**) Native pig skin; (**B**) SSG; (**C**) PG-PSE matured in serum-free media; and (**D**) PG-PSE matured in serum media were analysed using Masson's Trichrome (MT) staining to assess collagen deposition. Scale bar = 1 mm. Representative regions of the superficial neo-dermis (green) and deep neo-dermis (red) are indicated. Scale bar = 100 µm. (**E**) Collagen deposition in superficial and (**F**) deep neo-dermis was normalised against host native pig skin and analysed using one-way ANOVA, $p \leq 0.05$ (*), $p \leq 0.01$ (**), and $p \leq 0.001$ (***), N = 2 pigs; 3 grafts per treatment group per animal; superficial and deep neo-dermis areas from 6mm punch biopsy per graft were visualised. Six random ROI per superficial and deep neo-dermis per graft were analysed. Abbreviations: SSG: split skin graft; PG-PSE: Platelet hydroGel–Pig Skin Equivalent. ROI: region of interest.

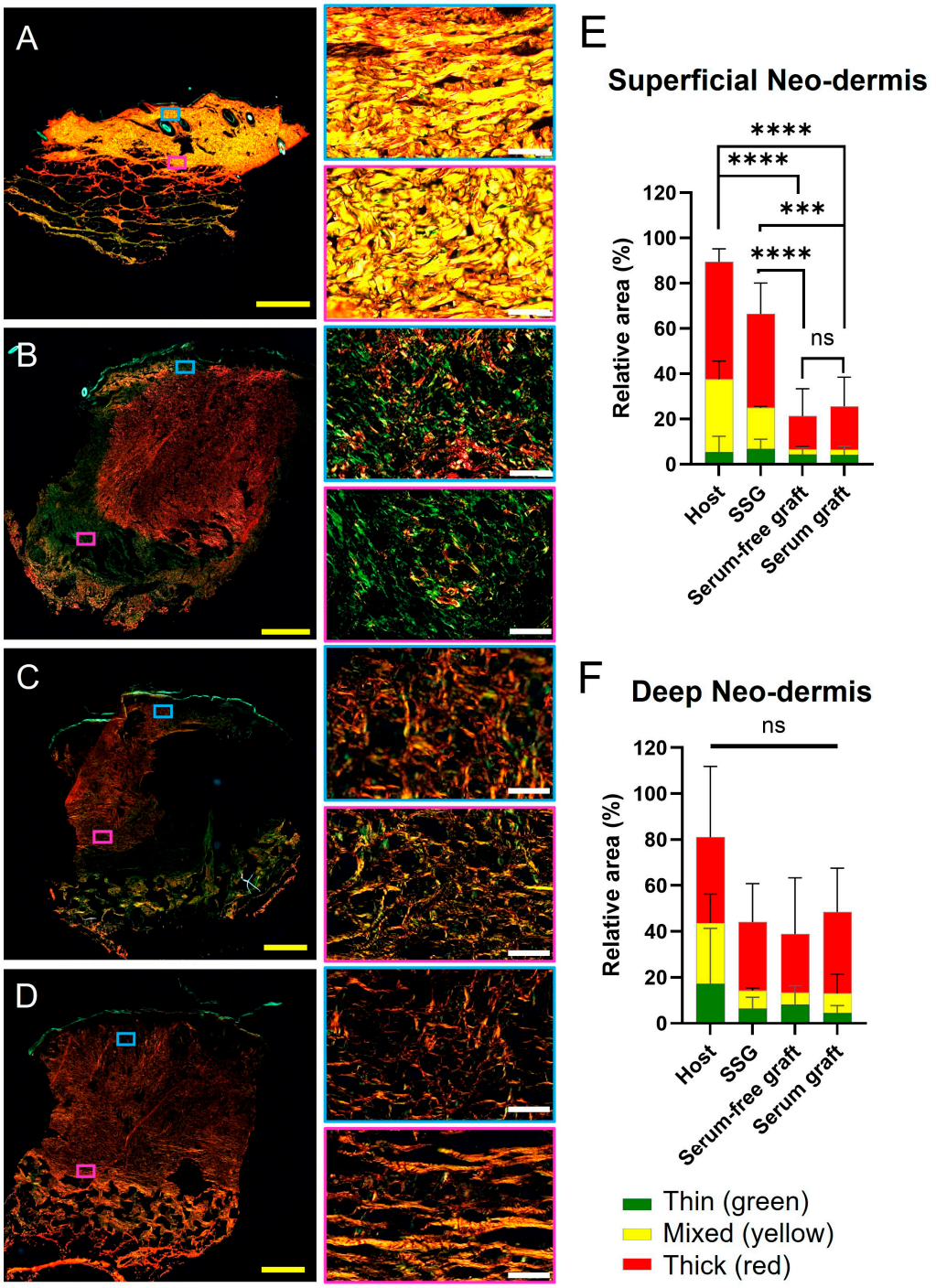


Figure 7. Picrosirius red (PSR) staining for collagen composition and arrangement in engineered grafts. (**A**) Native pig skin, (**B**) SSG, (**C**) PG-PSE matured in serum-free media, and (**D**) PG-PSE matured in serum-supplemented media 14 days post-grafting were stained with PSR. Scale bar = 1 mm. Enlarged regions are representative areas of superficial neo-dermis (light blue border), and deep neo-dermis (magenta border). Scale bar = 50 µm. (**E**) Collagen was quantified by type in superficial neo-dermis, (**F**) deep neo-dermis and normalised to the entire field of view. Statistical significance for quantified collagen is only indicated for type 1 collagen signal where $p \leq 0.001$ (***), $p \leq 0.0001$ (****) and ns (not significant) using one-way ANOVA. No further significant differences were identified otherwise. N = 2 pigs; 3 grafts per treatment group per animal; whole superficial and deep neo-dermis area in 6 mm punch biopsy per graft were visualised. Five ROI in superficial and five ROI in deep neo-dermis per graft were analysed. Abbreviations: SSG: split skin graft; PG-PSE: Platelet hydroGel–Pig Skin Equivalent, ROI: region of interest.

4. Discussion

In this feasibility study, we developed a large white pig model to evaluate the repair of large full-thickness wounds using bioengineered skin grafts. The bioengineered skin is prepared from autologous fibroblasts and keratinocytes and a bioactive hydrogel as the scaffold. In this model, the bioengineered skin graft was compared to the gold-standard native meshed SSG in terms of neo-epidermisation, vascularisation, and graft integration/remodelling.

Epidermal stratum corneum, stratum granulosum, stratum spinosum and stratum basale layers were detected in bioengineered skin graft, similar to the gold-standard meshed SSG, albeit thicker than uninjured skin. Thickened epidermis in all skin grafts has also been reported by transplantation of other bioengineered skin in pig models [5], consistent with increased keratinocyte proliferation during graft integration. CK5 expression was expanded to suprabasal layers in bioengineered skin grafts and meshed SSG, compared to uninjured skin, reflecting enrichment of proliferating keratinocytes during skin graft integration and remodelling [18]. Similarly, a study by Yamaguchi et al. has showed increased number of proliferative Ki67$^+$ keratinocyte in skin grafts [19]. The proliferating keratinocytes were supported by abundance of vimentin$^+$ fibroblasts in regenerated neo-dermis.

Two variants of PG-PSE were analysed in this study. Platelet lysate was tested to replace foetal calf serum during skin maturation in culture. Notably, both types of PG-PSE grafts, regardless of culture condition, formed rete ridges within two weeks post-grafting, reflecting progressive maturation of the neo-dermis and dermal–epidermal junction [20]. Rete ridges contribute to the mechanical integrity of skin by enhancing resistance to shear forces at the dermal–epidermal junction in pigs. In contrast, rodents and other loose-skinned animals in general lack rete ridges and exhibit a relatively flat dermal–epidermal interface [2]. Rete ridges were absent in the bioengineered skin that was grafted in a nude mouse model in an earlier study [7].

Timely vascularisation is fundamental to graft survival and graft integration, yet excessive vascularisation is associated with long-term fibrosis. Wounds grafted with both PG-HSE variants were fully vascularised in 2 weeks. Interestingly, we observed higher number and thicker microvessels in PG-PSE superficial neo-dermis, when PG-PSE was matured in platelet lysate (serum-free) during culture. The superior vessel density observed in serum-free, PL-supplemented conditions suggests that platelet lysate provides a supportive environment for neovascularisation immediately beneath the neo-epidermis, although serum-matured PG-HSE promoted more extensive vasculature in deep neo-dermis. The functional scarring consequences of having increased vascularisation is to be determined in a longer study.

We had previously studied physical and biochemical properties of PG hydrogel and showed that once PG is developed further into a live bioengineered skin, it closes wounds in an immune-compromised nude mouse model [7,21]. This study on a large animal, however, presents an independent animal model, providing further evidence for its feasibility to clinical translation. This study describes a two-stage procedure, that mimics skin grafting in clinics, by grafting full-thickness wounds with an acellular dermal template, followed by definitive wound closure with a bioengineered skin graft.

A major limitation of this study is the small number of animals grafted. However, incorporation of an internal control in the study design has reduced the effect of pig-to-pig variation when interpreting the data and has allowed a direct comparison between the treatment and the control. A consideration for small animal number is the complex nature of surgical procedure in this study which limits the feasibility of a large sample size. Nevertheless, the findings in this study remain indicative until validated in a larger cohort.

Collagen deposition, types and distribution in bioengineered skin grafts were fully analysed using Masson's trichrome and Picrosirius red staining. By two weeks post-skin grafting, similar ratio of thick/mixed (red and yellow fibres) and thin (green fibres) is reached in deep dermis, compared to uninjured skin, albeit at lower levels. However, in more superficial neo-dermis, there is still a lower level of thick/mixed (red and yellow) fibres in PG-PSE compared to SSG and native skin. This data suggests fresh collagen deposition in superficial neo-dermis in PG-PSE grafts is active and therefore collagen deposition and integration phase may be extended in PG-PSE grafts compared to native SSG. Longer-term studies are required to evaluate dermal mechanical stability, contraction, and tissue remodelling post-PG-PSE grafting. Investigation is also needed to determine whether slow collagen deposition in PG-PSE is any indication of reduced long-term risk of pathological fibrosis or hypertrophic scarring in these grafts.

In accordance with good manufacturing practice (GMP) guidelines, foetal calf serum was replaced with platelet lysate during PG-PSE maturation, eliminating any animal-derived component from the final stage of production. Further studies are underway to achieve full removal of foetal calf serum throughout the entire manufacturing process. Other bioengineered composite skin grafts under development such as denovoSkin™ (Cutiss AG, Schlieren, Switzerland) and SASS (LOEX, Quebec City, QC, Canada) also demonstrate the potential of autologous bioengineered skin grafts. However, our novel bioengineered skin has several advantages: unlike bovine collagen-based hydrogel in denovoSkin, PG-HSE has a unique human platelet hydrogel scaffold with inherent provascularisation and pro-epidermisation components [21,22]. Moreover, PG-HSE, similar to other platelet-derived materials, is beneficial in possessing antimicrobial activity [6,23]. PG-HSE is rapidly prepared, requiring 3 weeks for a scaled-up production, in comparison to SASS, which requires 6 weeks to prepare from a small skin biopsy and requires foetal calf serum during production [24]. This is a clinically significant advantage in a setting where time to wound healing has major survival, scarring and cost implications.

The bioengineered skin was generated by the timely expansion of autologous dermal fibroblasts and epidermal progenitor keratinocytes. Grafted autologous keratinocytes were subsequently traced within the regenerated epidermis, providing direct evidence of their engraftment leading to skin regeneration. Importantly, real-time production aligns well with the two-stage clinical management of deep wounds, in which a dermal template, such as BTM, is applied as the first step prior to definitive epidermal coverage [25]. This autologous bioengineered skin has also been proven to be effective in closing large wounds in a child with extensive burns [26].

5. Conclusions

Collectively, these data demonstrate the feasibility of scalable, clinically relevant production of autologous bioengineered skin for the treatment of large full-thickness wounds. It provides some clinically meaningful evidence for the effective repair of deep wounds with the novel autologous bioengineered skin and has potential applications in treating extensive skin defects, such as severe burns, reconstructive surgical defects, and giant congenital melanocytic nevi.

In addition, this pig model can be used to investigate the cellular and molecular pathways involved in wound repair following skin grafting. Improved understanding of the mechanisms governing wound repair and regeneration can support future advances in skin bioengineering.

Supplementary Materials: The following supporting information can be downloaded at https://www.mdpi.com/article/10.3390/bioengineering13111307/s1, Supplementary Data S1: Surgical procedures; Supplementary Data S2: In vitro labelling strategy.

Author Contributions: Conceptualisation, S.A., I.B., M.M.R., C.L.A. methodology, S.A., I.B., M.M.R.; software, I.B., M.M.R., C.L.A., P.A., S.L.W.W.; validation, S.A., I.B., M.M.R., C.L.A., P.A.; formal analysis, I.B., M.M.R., C.L.A., P.A., S.L.W.W., S.A.; investigation, S.A., I.B., M.M.R., C.L.A., P.A., H.C., C.H.L.; resources, D.C.M.; data curation, I.B., M.M.R., C.L.A., P.A., S.L.W.W.; writing—original draft preparation, S.A., I.B., C.L.A., S.L.W.W.; writing—review and editing, S.A., I.B., M.M.R., C.L.A., D.C.M., P.A., H.C., C.H.L.; visualisation, I.B., M.M.R., C.L.A., P.A., S.L.W.W.; supervision, S.A., H.C. All authors have read and agreed to the published version of the manuscript.

Funding: This research was funded by the Medical Research Future Fund—Rare Cancers, Rare Diseases and Unmet Need (application # MRF2006351).

Institutional Review Board Statement: The animal study protocol was approved by the Alfred Research Alliance Animal Ethics Committee (reference # P11678, 2 May 2025).

Informed Consent Statement: Not applicable.

Data Availability Statement: Data is contained within the article and Supplementary Material.

Acknowledgments: We thank Monash Histology Platform for their assistance with histological staining, Precinct Animal Centre (PAC) for animal care and Monash Micro Imaging (MMI) for their assistance with microscopy.

Conflicts of Interest: Authors declare no conflicts of interest.

Abbreviations

The following abbreviations are used in this manuscript:

BrdU	5-bromo-2′-deoxyuridine
EdU	5-Ethynyl-2′-deoxyuridine
MT	Masson's Trichrome
ROI	Region of interest.
SSG	Split thickness skin graft
PG-PSE	Platelet hydroGel-Pig Skin Equivalent

References

1. Meyer, W.; Schwarz, R.; Neurand, K. The skin of domestic mammals as a model for the human skin, with special reference to the domestic pig. *Curr. Probl. Dermatol.* **1978**, *7*, 39–52. [CrossRef] [PubMed]
2. Sullivan, T.P.; Eaglstein, W.H.; Davis, S.C.; Mertz, P. The pig as a model for human wound healing. *Wound Repair Regen.* **2001**, *9*, 66–76. [CrossRef] [PubMed]
3. Braye, F.M.; Stefani, A.; Venet, E.; Pieptu, D.; Tissot, E.; Damour, O. Grafting of large pieces of human reconstructed skin in a porcine model. *Br. J. Plast. Surg.* **2001**, *54*, 532–538. [CrossRef] [PubMed]
4. Dearman, B.L.; Stefani, K.; Li, A.; Greenwood, J.E. "Take" of a polymer-based autologous cultured composite "skin" on an integrated temporizing dermal matrix: Proof of concept. *J. Burn. Care Res.* **2013**, *34*, 151–160. [CrossRef] [PubMed]
5. Schiestl, C.; Biedermann, T.; Braziulis, E.; Hartmann-Fritsch, F.; Bottcher-Haberzeth, S.; Arras, M.; Cesarovic, N.; Nicolls, F.; Linti, C.; Reichmann, E.; et al. Skingineering II: Transplantation of large-scale laboratory-grown skin analogues in a new pig model. *Pediatr. Surg. Int.* **2011**, *27*, 249–254. [CrossRef] [PubMed]
6. Banakh, I.; Rahman, M.M.; Arellano, C.L.; Marks, D.C.; Mukherjee, S.; Gargett, C.E.; Cleland, H.; Akbarzadeh, S. Platelet lysate can support the development of a 3D-engineered skin for clinical application. *Cell Tissue Res.* **2023**, *391*, 173–188. [CrossRef] [PubMed]
7. Rahman, M.M.; Arellano, C.L.; Banakh, I.; Marks, D.C.; Carmichael, I.; Arfuso, F.; Lo, C.H.; Cleland, H.; Akbarzadeh, S. Bioengineered Skin from a Platelet-Derived Hydrogel Repairs Full Thickness Wounds in a Pre-Clinical Mouse Model. *Int. J. Mol. Sci.* **2025**, *26*, 9988. [CrossRef] [PubMed]

8. Lequeux, C.; Oni, G.; Wong, C.; Damour, O.; Rohrich, R.; Mojallal, A.; Brown, S.A. Subcutaneous fat tissue engineering using autologous adipose-derived stem cells seeded onto a collagen scaffold. *Plast. Reconstr. Surg.* **2012**, *130*, 1208–1217. [CrossRef] [PubMed]
9. Tondato, F.; Robinson, K.; Cui, J.; Goodchild, T.; Chronos, N.; Peters, N.S. Effects on arrhythmogenesis and arrhythmic threshold of injection of autologous fibroblasts into myocardial infarcts in adult pigs. *J. Cardiovasc. Transl. Res.* **2012**, *5*, 337–344. [CrossRef] [PubMed]
10. Lo, C.H.; Brown, J.N.; Dantzer, E.J.G.; Maitz, P.K.M.; Vandervord, J.G.; Wagstaff, M.J.D.; Barker, T.M.; Cleland, H. Wound healing and dermal regeneration in severe burn patients treated with NovoSorb(R) Biodegradable Temporising Matrix: A prospective clinical study. *Burns* **2022**, *48*, 529–538. [CrossRef] [PubMed]
11. Greenwood, J.E.; Dearman, B.L. Split skin graft application over an integrating, biodegradable temporizing polymer matrix: Immediate and delayed. *J. Burn. Care Res.* **2012**, *33*, 7–19. [CrossRef] [PubMed]
12. Vennin, C.; Melenec, P.; Rouet, R.; Nobis, M.; Cazet, A.S.; Murphy, K.J.; Herrmann, D.; Reed, D.A.; Lucas, M.C.; Warren, S.C.; et al. CAF hierarchy driven by pancreatic cancer cell p53-status creates a pro-metastatic and chemoresistant environment via perlecan. *Nat. Commun.* **2019**, *10*, 3637. [CrossRef] [PubMed]
13. Bankhead, P.; Loughrey, M.B.; Fernandez, J.A.; Dombrowski, Y.; McArt, D.G.; Dunne, P.D.; McQuaid, S.; Gray, R.T.; Murray, L.J.; Coleman, H.G.; et al. QuPath: Open source software for digital pathology image analysis. *Sci. Rep.* **2017**, *7*, 16878. [CrossRef] [PubMed]
14. Flomerfelt, F.A.; Gress, R.E. Analysis of Cell Proliferation and Homeostasis Using EdU Labeling. *Methods Mol. Biol.* **2016**, *1323*, 211–220. [CrossRef] [PubMed]
15. Salic, A.; Mitchison, T.J. A chemical method for fast and sensitive detection of DNA synthesis in vivo. *Proc. Natl. Acad. Sci. USA* **2008**, *105*, 2415–2420. [CrossRef] [PubMed]
16. Bruen, K.J.; Campbell, C.A.; Schooler, W.G.; de Serres, S.; Cairns, B.A.; Hultman, C.S.; Meyer, A.A.; Randell, S.H. Real-time monitoring of keratin 5 expression during burn re-epithelialization. *J. Surg. Res.* **2004**, *120*, 12–20. [CrossRef] [PubMed]
17. Rajaram, R.; Zhang, M.; Premaratne, G.; Ng, S. Novosorb((R)) BTM- history, production and application in challenging wounds. *Front. Bioeng. Biotechnol.* **2024**, *12*, 1450973. [CrossRef] [PubMed]
18. Debeer, S.; Le Luduec, J.B.; Kaiserlian, D.; Laurent, P.; Nicolas, J.F.; Dubois, B.; Kanitakis, J. Comparative histology and immunohistochemistry of porcine versus human skin. *Eur. J. Dermatol.* **2013**, *23*, 456–466. [CrossRef] [PubMed]
19. Yamaguchi, Y.; Hosokawa, K.; Kawai, K.; Inoue, K.; Mizuno, K.; Takagi, S.; Ohyama, T.; Haramoto, U.; Yoshikawa, K.; Itami, S. Involvement of keratinocyte activation phase in cutaneous graft healing: Comparison of full-thickness and split-thickness skin grafts. *Dermatol. Surg.* **2000**, *26*, 463–469. [CrossRef] [PubMed]
20. Kiwanuka, E.; Hackl, F.; Philip, J.; Caterson, E.J.; Junker, J.P.; Eriksson, E. Comparison of healing parameters in porcine full-thickness wounds transplanted with skin micrografts, split-thickness skin grafts, and cultured keratinocytes. *J. Am. Coll. Surg.* **2011**, *213*, 728–735. [CrossRef] [PubMed]
21. Rahman, M.M.; Garcia, N.; Loh, Y.S.; Marks, D.C.; Banakh, I.; Jagadeesan, P.; Cameron, N.R.; Yung-Chih, C.; Costa, M.; Peter, K.; et al. A platelet-derived hydrogel improves neovascularisation in full thickness wounds. *Acta Biomater.* **2021**, *136*, 199–209. [CrossRef] [PubMed]
22. Meuli, M.; Hartmann-Fritsch, F.; Huging, M.; Marino, D.; Saglini, M.; Hynes, S.; Neuhaus, K.; Manuel, E.; Middelkoop, E.; Reichmann, E.; et al. A Cultured Autologous Dermo-epidermal Skin Substitute for Full-Thickness Skin Defects: A Phase I, Open, Prospective Clinical Trial in Children. *Plast. Reconstr. Surg.* **2019**, *144*, 188–198. [CrossRef] [PubMed]
23. Shariati, A.; Moradabadi, A.; Azimi, T.; Ghaznavi-Rad, E. Wound healing properties and antimicrobial activity of platelet-derived biomaterials. *Sci. Rep.* **2020**, *10*, 1032. [CrossRef] [PubMed]
24. Germain, L.; Larouche, D.; Nedelec, B.; Perreault, I.; Duranceau, L.; Bortoluzzi, P.; Beaudoin Cloutier, C.; Genest, H.; Caouette-Laberge, L.; Dumas, A.; et al. Autologous bilayered self-assembled skin substitutes (SASSs) as permanent grafts: A case series of 14 severely burned patients indicating clinical effectiveness. *Eur. Cell. Mater.* **2018**, *36*, 128–141. [CrossRef] [PubMed]
25. Lo, C.H.; Wagstaff, M.J.D.; Barker, T.M.; Damkat-Thomas, L.; Salerno, S.; Holden, D.; Concannon, E.; Heath, K.; Coghlan, P.; Cleland, H. Long-term scarring outcomes and safety of patients treated with NovoSorb® Biodegradable Temporizing Matrix (BTM): An observational cohort study. *JPRAS Open* **2023**, *37*, 42–51. [CrossRef] [PubMed]
26. Akbarzadeh, S.; Zvi, E.; Arellano, C.L.; Banakh, I.; Rahman, M.M.; Marks, D.C.; Lo, C.H.; Boyce, S.T.; Bertinetti, M.; Teague, W.; et al. A novel engineered skin closes full thickness burn wounds: A case report. *JPRAS Open* **2026**, *49*, 479–486. [CrossRef] [PubMed]

Disclaimer/Publisher's Note: The statements, opinions and data contained in all publications are solely those of the individual author(s) and contributor(s) and not of MDPI and/or the editor(s). MDPI and/or the editor(s) disclaim responsibility for any injury to people or property resulting from any ideas, methods, instructions or products referred to in the content.